Radar Based Humans Localization with Compressed Sensing and Sparse Reconstruction

(Invited Paper)

Christian Eckrich*†, Christian A. Schroth*, Vahid Jamali† and Abdelhak M. Zoubir*
*Signal Processing Group, †Resilient Communication Systems
Technische Universität Darmstadt, Germany
*{eckrich, schroth, zoubir}@spg.tu-darmstadt.de, †{christian.eckrich, vahid.jamali}@rcs.tu-darmstadt.de

***Abstract*—Localization and detection is a vital task in emergency rescue operations. Devastating natural disasters can create environments that are inaccessible or dangerous for human rescuers. Contaminated areas or buildings in danger of collapsing can be searched by rescue robots which are equipped with diverse sensors such as optical and radar sensors. In scenarios where the line of sight is blocked, e.g., by a wall, a door or heavy smoke or dust, sensors like LiDAR or cameras are not able to provide sufficient information. The usage of radar in these kinds of situations can drastically improve situational awareness and hence the likelihood of rescue. In this paper, we present a method that is used for radar imaging behind obstacles by utilizing a signal model that includes the floor reflection propagation path in addition to the direct path of the radar signal. Additionally, compressed sensing methods are presented and applied to real world radar data that was recorded by a Stepped Frequency Continuous Wave (SFCW) radar mounted on a semi-autonomous robot. The results show an improved radar image that allows the clear identification of persons behind obstacles.**

***Keywords*—sparse reconstruction, compressed sensing, multipath exploitation, SFCW radar, localization, semi-autonomous robot**

I. Introduction

The utilization of radar in locating humans in emergency scenarios is of high importance when the visibility is restricted, and optical sensors, e.g., light detection and ranging (LiDAR), RGB- or infrared cameras, cannot be applied. Typical obstacles that impact the line of sight are walls, doors or heavy smoke. In a scenario where humans must be found in an area that is inaccessible to rescuers, the usage of rescue robots (such as the semi-autonomous emergenCITY robot 'Scout' shown in Fig. 1) is advantageous [1], [2]. It allows to reliably navigate in environments that are contaminated or buildings that are in danger of collapsing after a natural disaster. Rescue robots can be equipped with a variety of different sensors, including radar sensors that, unlike optical sensors, are applicable even when the line of sight is blocked. Radar imaging through an obstacle, like a wall, has been investigated in [3], [4] and [5], while the authors in [6] proposed an iterative target detection scheme. The detection performance depends on the characteristics of the utilized radar system, which is discussed and evaluated in [7]. The authors in [8] and [9] used a Stepped Frequency Continuous Wave (SFCW) radar system with a large antenna aperture to detect and classify targets behind walls. The suppression of ghost images resulting from signal reflections due to side walls and wall ringing effects has been investigated in [10].

Compressed sensing (CS) is a technique that exploits the sparsity of a signal to reconstruct it from a limited number of measurements [11]. It can reduce the computational cost and fasten the collection of radar data. This is necessary for real world applications when lives are at risk and the emergenCITY robot has limited time for the search of missing persons. In this paper, we use the robot's onboard Walabot multiple-input multiple-output (MIMO) radar developed by vayyar[1] for radar imaging and humans localization. We apply compressed sensing methods and utilize the signal components that result from reflections with the floor in order to enhance the three-dimensional (3D) image quality. A sparsifying base utilizing the 3D Dual-Tree Complex Wavelet Transform (DT-CWT) models the spatial extension of the human body and allows relaxing the unrealistic point target assumption [11]. The presented results are based on real world data captured by the radar of the emergenCITY robot in an experiment that emulates different radar imaging scenarios of various persons behind obstacles in different postures and locations.

Fig. 1: emergenCITY robot 'Scout'

The remainder of this paper is organized as follows. In Sections II and V-A, the signal model is introduced and fundamentals of radar imaging are briefly revisited. The compressed sensing approach is shown in Section III and the group sparse problem formulation is presented in Section IV. Sections V and V-B give an overview of the setup of the conducted experiments and present the obtained results. Finally, conclusions are drawn in Section VI.

II. Signal Model

The 3D-space, observed by an SFCW radar, is partitioned into $G = G_x G_y G_z$ grid cells, where G_x, G_y and G_z are the number of grid cells in each spatial dimension. The position of each grid cell is given by $\boldsymbol{g} = [g_x, g_y, g_z]^\top$. Let $\boldsymbol{e}_x$, $\boldsymbol{e}_y$, and $\boldsymbol{e}_z$ denote the standard bases for the 3D space. The radar transmit and receive antennas are distributed in the plane spanned by $\boldsymbol{e}_x$ and $\boldsymbol{e}_y$ at positions $\boldsymbol{m}_{\text{tx}}$ and $\boldsymbol{m}_{\text{rx}}$, respectively. The floor is located at $y = 0$ and spanned by $\boldsymbol{e}_x$ and $\boldsymbol{e}_z$. A sketch of the radar setup can be seen in Fig. 2.

The transmit antennas radiate (each at a time), a stepped frequency signal with frequency steps $f_k = f_0 + k\Delta f$ for $k = 0, \ldots, K-1$. During the transmission period of each transmit antenna, all receive antennas record the returning signal[2]. In other words, we record a signal for each pair of transmit and receive antennas. It is assumed that the radar scene is stationary between the activation of

[1] https://vayyar.com

[2] The described radar scanning protocol is pre-programmed by the used radar and hence cannot be changed in our experiments.

979-8-3503-3959-8/23/$31.00 ©2023 IEEE

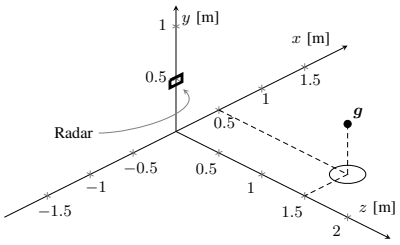

Fig. 2: Global coordinate system of the observed space.

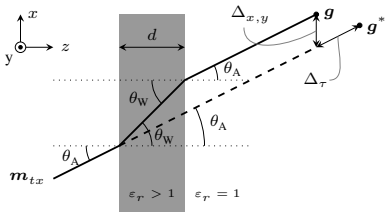

Fig. 3: Refraction of the EM wave at the surface of a medium.

the first and last transmit antenna. The combination of each transmit antenna and each receive antenna results in M antenna pairs, each corresponding to a received fast time signal. The signal strength can be modelled by the signal energy $\boldsymbol{\sigma} = [\sigma_0, \ldots, \sigma_{G-1}]^\top \in \mathbb{C}^{G\times 1}$ reflected from G grid cells. The reflected signal from each grid cell is allocated a time shift τ_{gm} due to the duration needed for the electromagnetic (EM) wave to travel from the transmit antenna to the reflecting grid cell $\boldsymbol{g}$ and back to the receive antenna. The summation over the signal originating from each grid cell $\boldsymbol{g}$ leads to the construction of the total receive signal for antenna pair m and frequency step k [12]. However, in many cases, the returning signal is not limited to the direct path between the grid cell and the radar. Multipath propagation is a common observation in real radar recordings. In particular, the reflection from the floor is one of the dominant multi-path components and hence is explicitly accounted for in our signal model. This leads to the introduction of a mirror image indicated by $\boldsymbol{\sigma}' = [\sigma'_0, \ldots, \sigma'_{G-1}]^\top \in \mathbb{C}^{G\times 1}$ and the corresponding time shift τ'_{gm} that represents the delay via the reflection from the ground. The total received signal including the floor multipath propagation can be expressed as

$$z(k,m) = \sum_{g=0}^{G-1} \left(\sigma_g \, e^{-j2\pi f_k \tau_{gm}} + \sigma'_g \, e^{-j2\pi f_k \tau'_{gm}} \right) + \varepsilon_{km}. \quad (1)$$

The entries of the measurement vector $\boldsymbol{z} \in \mathbb{C}^{KM\times 1}$ are composed of $z(k,m)$ as

$$\boldsymbol{z} = \mathrm{vec}\left([\boldsymbol{z}_0, \ldots, \boldsymbol{z}_{M-1}]\right), \quad \text{with} \quad (2)$$

$$\boldsymbol{z}_m = [z(0,m), \ldots, z(K-1,m)]^\top \in \mathbb{C}^{K\times 1} \quad (3)$$
$$\text{for} \quad m = 0, \ldots, M-1,$$

where $\mathrm{vec}(\cdot)$ represent a vectorizing operator that stacks the columns of a matrix into a vector. In matrix notation, $\boldsymbol{z}$ can be expressed as

$$\boldsymbol{z} = \boldsymbol{\Psi}\boldsymbol{\sigma} + \boldsymbol{\Psi}'\boldsymbol{\sigma}' + \boldsymbol{\varepsilon}, \quad (4)$$

where $\boldsymbol{\Psi}, \boldsymbol{\Psi}' \in \mathbb{C}^{KM\times G}$ are the direct path and the floor path propagation models and $\boldsymbol{\varepsilon} = [\varepsilon_0, \ldots, \varepsilon_{KM-1}]^\top \in \mathbb{C}^{KM\times 1}$ represents additive white Gaussian noise and clutter components. The image vectors $\boldsymbol{\sigma}, \boldsymbol{\sigma}'$ can be seen as a 3D map of the scene observed by the radar. The objective is to reconstruct the map based on the radar recordings $\boldsymbol{z}$ and detect the location of humans. The time delay for the direct path correlates with the summation of the Euclidean distance between the position of the transmit antenna $\boldsymbol{m}_{\text{tx}}$ and the position of the grid cell $\boldsymbol{g}$, and the Euclidean distance between the position of the grid cell $\boldsymbol{g}$ and the position of the receive antenna $\boldsymbol{m}_{\text{rx}}$. The time delays are given by

$$\tau_{gm} = \frac{1}{c_0}||\boldsymbol{m}_{\text{tx}} - \boldsymbol{g}||_2 + \frac{1}{c_0}||\boldsymbol{m}_{\text{rx}} - \boldsymbol{g}||_2 \quad \text{and} \quad (5)$$

$$\tau'_{gm} = \frac{1}{c_0}||\boldsymbol{m}_{\text{tx}} - \boldsymbol{g}||_2 + \frac{1}{c_0}\left\| \left([1,-1,1]^\top \odot \boldsymbol{m}_{\text{rx}} \right) - \boldsymbol{g} \right\|_2, \quad (6)$$

where $\odot$ is the Hadamard multiplication and c_0 is the speed of light in air. The path that leads to τ'_{gm} is composed of the direct path between $\boldsymbol{m}_{\text{tx}}$ and $\boldsymbol{g}$, and the path between $\boldsymbol{g}$ and the virtual receive antenna whose position is mirrored at the floor. The power via the path $\boldsymbol{m}_{\text{tx}}$-floor-$\boldsymbol{g}$-$\boldsymbol{m}_{\text{rx}}$ is expected to be much weaker than the direct path $\boldsymbol{m}_{\text{tx}}$-$\boldsymbol{g}$-$\boldsymbol{m}_{\text{rx}}$, while both are impinging on the receive antennas from the same angles. Therefore, we neglect $\boldsymbol{m}_{\text{tx}}$-floor-$\boldsymbol{g}$-$\boldsymbol{m}_{\text{rx}}$ and only consider $\boldsymbol{m}_{\text{tx}}$-$\boldsymbol{g}$-floor-$\boldsymbol{m}_{\text{rx}}$ in addition to the direct path.

A. Positioning Error Caused by Obstacles

The path between the radar and the object can be obstructed by a medium with permeability $\varepsilon_r > 1$ and width d, e.g., a wall or a door. For simplicity, the medium is orientated in parallel to the y-x plane and the antenna array. The propagating EM wave is diverted towards the surface normal on entry from air to the medium. Likewise, exiting the medium, the EM wave is diverted away from the surface normal. In order to account for the resulting positioning error, the obstacle's permeability and thickness has to be known. The wave refraction at the surface can be described by Snell's law,

$$\frac{\sin(\theta_{\text{A}})}{\sin(\theta_{\text{W}})} = \sqrt{\varepsilon_r}, \quad (7)$$

where θ_{A} and θ_{W} are the angles spanned between the surface's normal and the EM wave's path during outside and inside the medium, as shown in Fig. 3 [12]. Due to the refraction at the surface of the medium and the influence of ε_r on the EM wave's propagation speed, the grid cell $\boldsymbol{g}$ is observed by the radar to be at the position of $\boldsymbol{g}^*$. Hence, Eqs. (5) and (6) have to be updated with $\boldsymbol{g} \to \boldsymbol{g}^*$. The first position correction can be expressed as a shift in the x-y plane along the direction in which θ_W and θ_A opens. It is given by

$$\Delta_{x,y} = d\left(\tan(\theta_{\text{W}}) - \tan(\theta_{\text{A}})\right). \quad (8)$$

The second correction results from the elongated path and the reduced speed of light in a medium with $\varepsilon_r > 1$ and is given by

$$\Delta_\tau = d\left(\frac{\sqrt{\varepsilon_r}}{\cos(\theta_{\text{W}})} - \frac{1}{\cos(\theta_{\text{A}})}\right). \quad (9)$$

III. Compressed Sensing

In many cases, it is advantageous to reduce the number of recorded samples that are used to reconstruct the image vector $\boldsymbol{\sigma}$ and the corresponding 3D map. Thus, the computational complexity is reduced, and the estimation can be conducted faster. In general, the radar scene can be considered to be mostly empty. Only sporadic objects that are located in the scene lead to a peak in the image vector. Under this assumption $\boldsymbol{\sigma}$ and $\boldsymbol{\sigma}'$ can be considered to be sparse, e.g., the image vector has only $G_s \ll G$ non-zero entries. CS theory states that $\boldsymbol{\sigma}$ and $\boldsymbol{\sigma}'$ can be reconstructed using only a subsection of measurement observations sampled below the Nyquist rate. In real world application, the radar system would be adapted to record only $K_d M_d \ll KM$ data points. However, in the case of pre-recorded radar data, the introduction of a downsampling matrix $\boldsymbol{\Phi}$ is necessary. For the design of $\boldsymbol{\Phi}$, it is important that the significant part of the full image vectors $\boldsymbol{\sigma}$ and $\boldsymbol{\sigma}'$ are not in the null space of $\boldsymbol{\Phi}$. Using stepped frequency radar, an efficient sampling scheme has proven to be a binary downsampling matrix $\boldsymbol{\Phi} \in \{0,1\}$ of size $K_d M_d \times KM$ [13]. The unstructured downsampling matrix is constructed by randomly

choosing without replacement, denoted by $\in_R$, a random subset $\mathcal{F}_{\text{sub}} \in_R \{f_0, \ldots, f_{K-1}\}$ from the set of all frequencies so that the size of the subset $|\mathcal{F}_{\text{sub}}| = K_d$. Likewise, a random subset of antenna pairs is chosen as $\mathcal{M}_{\text{sub}} \in_R \{m_0, \ldots, m_{M-1}\}$ with $|\mathcal{M}_{\text{sub}}| = M_d$, where $|\cdot|$ is the cardinality of a set. Each row of $\boldsymbol{\Phi}$ has only one entry that is equal to 1 while all the other entries are 0. The non-zero entry of each row is the index of each combination between $\mathcal{F}_{\text{sub}}$ and $\mathcal{M}_{\text{sub}}$. The resulting model of the reduced measurement vector $\bar{\boldsymbol{z}}_i$ for the i-th realization of the random downsampling matrix $\boldsymbol{\Phi}_i$ is given by

$$\begin{aligned}\bar{\boldsymbol{z}}_i &= \boldsymbol{\Phi}_i \boldsymbol{z} + \boldsymbol{\varepsilon} \\ &= \boldsymbol{\Phi}_i(\boldsymbol{\Psi}\boldsymbol{\sigma} + \boldsymbol{\Psi}'\boldsymbol{\sigma}') + \boldsymbol{\varepsilon}_i,\end{aligned} \tag{10}$$

where ε_i is the noise of the sampled data. Because $\boldsymbol{\sigma}$ and $\boldsymbol{\sigma}'$ are sub images that are based on the same observed radar scene, the model expression can be condensed by collecting both sub image vectors in one tall image vector $\tilde{\boldsymbol{\sigma}}$. The resulting model is given by

$$\tilde{\boldsymbol{z}} = \tilde{\boldsymbol{\Phi}} \begin{bmatrix} \boldsymbol{\Psi} & \boldsymbol{\Psi}' \end{bmatrix} \begin{bmatrix} \boldsymbol{\sigma} \\ \boldsymbol{\sigma}' \end{bmatrix} + \tilde{\boldsymbol{\varepsilon}} = \tilde{\boldsymbol{\Phi}}\tilde{\boldsymbol{\Psi}}\tilde{\boldsymbol{\sigma}} + \tilde{\boldsymbol{\varepsilon}}, \tag{11}$$

where $\tilde{\boldsymbol{\Phi}}$ is a realization of the random downsampling matrix. In the presented model, the assumption has been made that $\boldsymbol{\sigma}$ is sparse by resembling point like objects. However, $\boldsymbol{\sigma}$ underlays some structure if the objects are extended in space. A sparsifying basis $\boldsymbol{\Psi}_w$ for that

$$\boldsymbol{\sigma} = \boldsymbol{\Psi}_w \boldsymbol{x} \quad \text{and} \quad \boldsymbol{\sigma}' = \boldsymbol{\Psi}_w \boldsymbol{x}', \tag{12}$$

has to be found. A suitable approach is a basis composed by using the 3D dual-tree complex wavelet transform (DT-CWT) [11]. The vector containing the wavelet coefficient $\boldsymbol{x} = [x_0, \ldots, x_{G-1}]^\top$ remains sparse, even for extended objects. Comparable to Eq. (11), the wavelet coefficients $\boldsymbol{x}$ can be stacked to form a tall coefficient vector $\tilde{\boldsymbol{x}} = \text{vec}\left([\boldsymbol{x}, \boldsymbol{x}']\right)$, leading to the signal model

$$\tilde{\boldsymbol{z}} = \tilde{\boldsymbol{\Phi}}\tilde{\boldsymbol{\Psi}}_w\tilde{\boldsymbol{x}} + \tilde{\boldsymbol{\varepsilon}}. \tag{13}$$

IV. Group Sparse Problem Formulation

The objective is to reconstruct the image vector $\tilde{\boldsymbol{\sigma}}$ by utilizing the reduced observation vector $\tilde{\boldsymbol{z}}$. In order to promote sparse solutions, the ℓ_1 norm is used as a penalty term. Note, that $\tilde{\boldsymbol{\sigma}}$ incorporates multiple versions of the same underling image observed through different paths. Therefore, the promotion of sparsity should account for the grouped structure of $\tilde{\boldsymbol{\sigma}}$. This can be accomplished by the $\ell_{2,1}$ norm, defined as

$$||\tilde{\boldsymbol{\sigma}}||_{2,1} = \sum_{g=0}^{G-1} \sqrt{(\sigma_g)^2 + (\sigma_g')^2}. \tag{14}$$

For noiseless observations, this leads to the reconstruction problem

$$\hat{\boldsymbol{\sigma}} = \arg\min_{\tilde{\boldsymbol{\sigma}}} ||\tilde{\boldsymbol{\sigma}}||_{2,1} \quad \text{s.t.} \quad \tilde{\boldsymbol{z}} = \tilde{\boldsymbol{\Phi}}\tilde{\boldsymbol{\Psi}}\tilde{\boldsymbol{\sigma}}. \tag{15}$$

Using the Lagrange multiplier and considering noise, the convex optimization problem can be formulated as

$$\hat{\boldsymbol{\sigma}} = \arg\min_{\tilde{\boldsymbol{\sigma}}} \frac{1}{2}||\tilde{\boldsymbol{z}} - \tilde{\boldsymbol{\Phi}}\tilde{\boldsymbol{\Psi}}\tilde{\boldsymbol{\sigma}}||_2^2 + \lambda||\tilde{\boldsymbol{\sigma}}||_{2,1}, \tag{16}$$

where $\lambda \in \mathbb{R}^+$ is a regularization parameter that balances between the sparsity of the solution and the fidelity of the measurements. Likewise, the group sparse reconstruction problem using the complex 3D DT-CWT can be expressed as

$$\hat{\boldsymbol{x}} = \arg\min_{\tilde{\boldsymbol{x}}} \frac{1}{2}||\tilde{\boldsymbol{z}} - \tilde{\boldsymbol{\Phi}}\tilde{\boldsymbol{\Psi}}_w\tilde{\boldsymbol{x}}||_2^2 + \lambda||\tilde{\boldsymbol{x}}||_{2,1}, \tag{17}$$

where

$$||\tilde{\boldsymbol{x}}||_{2,1} = \sum_{g=0}^{G-1} \sqrt{(x_g)^2 + (x_g')^2}. \tag{18}$$

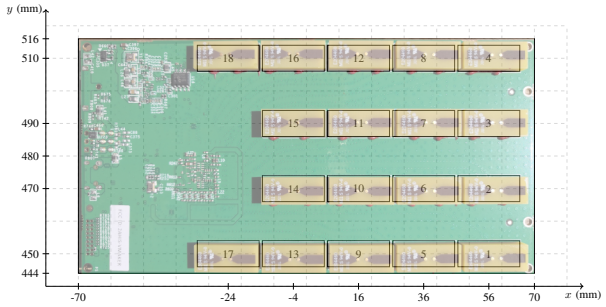

Fig. 4: Positions of the Walabot radar antennas in the global coordinate system from Fig. 2 with the radar's PCB in the background.

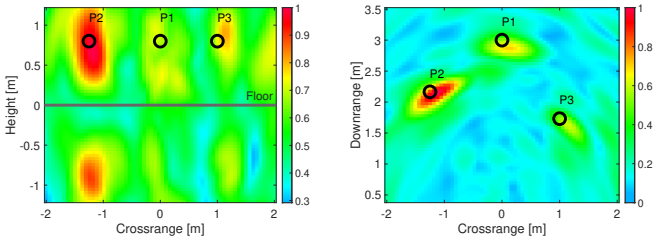

(a) Radar's perspective (b) Bird's eye view

Fig. 5: DSBF 3D map, recording with 3 persons.

Problems (16) and (17) can be solved using, e.g., the SpaRSA algorithm [14].

V. Experiments and Results

In an experiment, the onboard Walabot radar of the emergenCITY robot 'Scout' was used to record different radar scenes of sitting or laying persons. In each scene, 1-5 persons were located at an arbitrary location in front of the robot with a maximum radial distance of 3.5 m. The setup allowed the introduction of a 17.2 cm thick brick wall or a 2.5 cm wooden door between the radar and the persons [15]. The Walabot radar is a compact MIMO SFCW radar with 18 receive antennas, 4 of which can also function as transmit antennas. The dimensions and the positioning of the antennas is shown in Fig. 4. In this experiment the transmit antennas 1, 4, 17 and 18 are used while the receive signal is captured by receive antennas 2, 3, 6, 7, 10, 11, 14 and 15. This results in $M = 32$ transmit-receive antenna combinations. One radar sweep consists of $K = 137$ frequency steps ranging from 6.3 GHz to 8 GHz. The raw radar signal can include different clutter components, e.g, reflections from the wall, door or other stationary objects located in the observed space. However, due to the person's breathing, the stationary clutter signal can be removed by using a moving average filter with a length 5seconds, while maintaining the signal originating from the persons.

A. Delay and Sum Beamforming

By applying a conventional Delay and Sum Beamformer (DSBF), the received signal can be processed to steer towards each grid cell $\boldsymbol{g}$. The resulting complex image $r(g)$ is given by

$$r(g) = \frac{1}{KM} \sum_{m=0}^{M-1} \sum_{k=0}^{K-1} z(k,m) e^{j2\pi f_k \tau_{gm}} \tag{19}$$

and incorporates only the direct path between grid cell $\boldsymbol{g}$ and antenna m. The result can be seen as a 3D cost function, where the peaks indicate the origin of the reflected signal. In Fig. 5, the results of the DSBF are shown for a radar scene with three persons. The true locations for persons P1, P2, and P3 are indicated by the black circles.

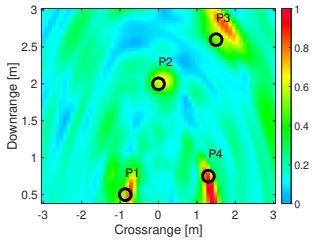

Fig. 6: DSBF of scene with four persons in free space.

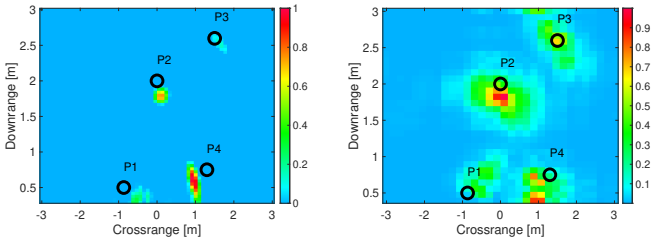

(a) Image reconstruction using point target assumption.

(b) Image reconstruction using DT-CWT.

Fig. 7: Bird's eye view of reconstructed 3D image with $\lambda = 0.4$. Recording of four persons in free space.

Fig. 5b depicts the bird's eye view of the scene. In Fig. 5a, the result is shown from the radar's perspective. The grid has been chosen to extend beneath the floor, which is located at $y = 0$. There are strong clusters of reflected signal energy that seem to be originating from below the floor. However, they relate to the signal received via the floor multi path. The resulting radar image is populated with numerous peaks. Only the three most prominent ones relate to a present person.

B. Results of the Proposed Method

In the sequel, the results using the proposed methods are shown and compared to the DSBF solution. Fig. 6 depicts the bird's eye view of the normalized 3D radar image resulting from the DSBF. The true positions of persons P1-P4 are marked by the black circles. It should be noted that person P2 is in a lying position whereas the other persons are sitting. Hence, P2 occupies a larger area in contrast to the sitting persons. In Fig. 7 the resulting bird's eye view of the normalized 3D radar image using the proposed method from Section IV is shown while utilizing all 32 antenna pairs and all 137 frequency steps. By evaluating different values for the regularization parameter λ, the value that achieves the best balance between image sparsity and measurement error was 0.4. Fig. 7a depicts the results based on the point target assumption from Eq. (16). Clusters have formed at the positions in which the persons were located, while the remaining area indicates no receive signal energy. The number of coefficients needed to represent the four persons in the 3D radar image is much higher than for the results depicted in Fig. 7b which utilize the DT-CWT to model the extended nature of persons in space. The depicted radar image is a solution of Eq. (17). Both methods found a sparse solution that is able to depict all present persons and, in contrast to the DSBF, suppress unwanted clutter components. This leads to an image that indicates the position of present persons in an undisturbed way. The degree of compressed sensing can be measured by the compressing ratio $R_{\text{CS}} = \frac{M_d K_d}{MK}$, where $M_d = \lceil \alpha M \rceil$ and $K_d = \lceil \alpha K \rceil$. The percentage of used antenna pairs and frequency bins is controlled by α. Hence, the ratio between K_d and M_d is approximately constant. Fig. 8b depicts the resulting bird's eye view of the normalized 3D radar image using the DT-CWT approach in a scenario of one person

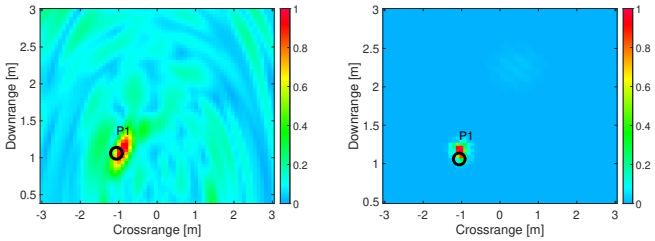

(a) DSBF image.

(b) Radar imaging (DT-CWT).

Fig. 8: Recording of one person behind door. Bird's eye view of 3D image with $\lambda = 0.6$ and $R_{\text{CS}} = 0.5$.

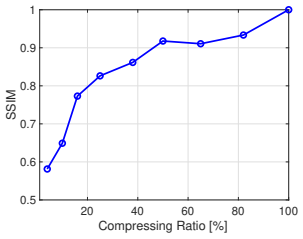

Fig. 9: Median SSIM for different compression rates in reference to the uncompressed case.

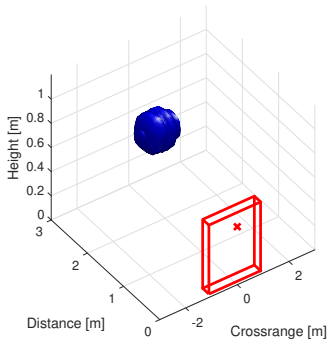

Fig. 10: Recording of one person at a distance of 2.5 m behind a wall with $\lambda = 0.6$ and $R_{\text{CS}} = 0.5$. A sketch of the wall's position is given in red.

sitting behind a wooden door at a distance of 1.5 m and an angle of -45°. The Regularization parameter λ has been set to 0.6 and $R_{\text{CS}} = 50\,\%$. The result using the DSBF for the same scene is given in Fig. 8a. The structural similarity index measure (SSIM) describes the structural similarity between two images. Using the SSIM metric, the resulting radar image for different R_{CS} has been evaluated. Fig. 9 shows the median SSIM value of 10 measurements with varying R_{CS}. It can be seen that decreasing the ratio beyond $30\,\%$ degrades the radar image quality drastically. However, utilizing between $50\,\%$ to $40\,\%$ of the radar data is a good balance between compression and image quality. This allows the computation time to be reduced and enable fast radar imaging that can be used in emergency scenarios. Fig. 10 depicts the 3D radar image of a person behind a wall at a distance of 2.5 m. The regularizing parameter λ was set to 0.8 and only $50\,\%$ of the available data was used. The depicted shape represents the isosurface of the pixels that exceed a threshold of 0.2. The wall and the position of the radar is illustrated in red.

VI. Conclusion

The application of CS methods in combination with a sparsifying DT-CWT basis has been demonstrated using experimental radar recordings of multiple persons behind obstacles. It has been shown that the compact Walabot radar with a limited antenna aperture is able to generate a precise image of the space behind the obstacle by utilizing the floor propagation multi path in addition to the direct path.

Acknowledgment

This work has been funded by LOEWE initiative (Hesse, Germany) within the emergenCITY centre.

REFERENCES

[1] M. Hollick, A. Hofmeister, J. I. Engels, *et al.*, "The Emergency Responsive Digital City," in *World Congress on Resilience, Reliability and Asset Management 2019*, 2019. [Online]. Available: https://www.sim.informatik.tu-darmstadt.de/publ/download/2019_emergenCITY_WCRRAM.pdf.

[2] I. Kruijff-Korbayova, R. Grafe, N. Heidemann, *et al.*, "German Rescue Robotics Center (DRZ): A Holistic Approach for Robotic Systems Assisting in Emergency Response," in *2021 IEEE International Symposium on Safety, Security, and Rescue Robotics (SSRR)*, IEEE, 2021, pp. 138–145.

[3] R. Kozlov, K. Gavrilov, T. Shevgunov, and V. Kirdyashkin, "Stepped-Frequency Continuous-Wave Signal Processing Method for Human Detection Using Radars for Sensing Rooms through the Wall," *Inventions*, vol. 7, no. 3, p. 79, 2022.

[4] Kusmadi and A. Munir, "Simulation design of compact stepped-frequency continuous-wave through-wall radar," in *2015 International Conference on Electrical Engineering and Informatics (ICEEI)*, IEEE, 2015, pp. 332–335.

[5] M. G. Amin, Ed., *Through-the-wall radar imaging*. Boca Raton, Fla., London, and New York, NY: CRC Press, 2011.

[6] C. Debes, J. Riedler, A. M. Zoubir, and M. G. Amin, "Adaptive target detection with application to through-the-wall radar imaging," *IEEE Transactions on Signal Processing*, vol. 58, no. 11, pp. 5572–5583, 2010.

[7] G. Paterniani, D. Sgreccia, A. Davoli, *et al.*, *Radar-based monitoring of vital signs: A tutorial overview*, Mar. 2022.

[8] C. Debes, J. Hahn, A. M. Zoubir, and M. G. Amin, "Target Discrimination and Classification in Through-the-Wall Radar Imaging," *IEEE Transactions on Signal Processing*, vol. 59, no. 10, pp. 4664–4676, 2011.

[9] C. Debes, M. G. Amin, and A. M. Zoubir, "Target Detection in Single- and Multiple-View Through-the-Wall Radar Imaging," *IEEE Transactions on Geoscience and Remote Sensing*, vol. 47, no. 5, pp. 1349–1361, 2009.

[10] M. Leigsnering, F. Ahmad, M. G. Amin, and A. M. Zoubir, "Multipath exploitation in through-the-wall radar imaging using sparse reconstruction," *IEEE Transactions on Aerospace and Electronic Systems*, vol. 50, no. 2, pp. 920–939, 2014.

[11] M. Leigsnering, C. Debes, and A. M. Zoubir, "Compressive sensing in through-the-wall radar imaging," in *2011 IEEE International Conference on Acoustics, Speech and Signal Processing (ICASSP)*, IEEE, 2011, pp. 4008–4011.

[12] M. Leigsnering, *Sparsity-Based Multipath Exploitation for Through-the-Wall Radar Imaging*, 2014.

[13] Y.-S. Yoon and M. G. Amin, "Compressed sensing technique for high-resolution radar imaging," in *Signal Processing, Sensor Fusion, and Target Recognition XVII*, SPIE, vol. 6968, 2008, pp. 506–515.

[14] S. J. Wright, R. D. Nowak, and M. A. T. Figueiredo, "Sparse reconstruction by separable approximation," *IEEE Transactions on Signal Processing*, vol. 57, no. 7, pp. 2479–2493, 2009.

[15] C. A. Schroth, C. Eckrich, I. Kakouche, *et al.*, "Emergency response person localization and vital signs estimation using semi-autonomous robot mounted sfcw radar," *(to be published)*,